特集 People Tracking with UWB Radar Using a Multiple-Hypothesis Tracking of Clusters (MHTC) Method*

光本直樹　SangHyun Chang　Michael Wolf　Joel W. Burdick
Naoki MITSUMOTO

This paper presents a method to track multiple moving humans using Ultra-Wideband (UWB) radar. UWB radar can complement other human tracking technologies, as it works well in poor visibility conditions. Our tracking approach is based on a point process interpretation of the multi-path UWB radar scattering model for moving humans. Based on this model, we present a multiple hypothesis tracking (MHT) framework for tracking the ranges and velocities of a variable number of moving human targets. The multi-target tracking (MTT) problem for UWB radar differs from traditional applications because of the complex multipath scattering per target. We develop an MHT framework for UWB radar-based multiple human target tracking, which can simultaneously solve the complex data association and tracking problems using Bayesian inference. We present experimental results in which a monostatic UWB radar tracks both individual and multiple human targets, even with changing numbers of targets across radar scans.

Key words：UWB radar, human tracking, multi-target tracking, multiple hypothesis tracking

1. Introduction

This paper explores the use of Ultra-Wideband (UWB) radar for tracking multiple moving humans. Because the ability to track human movement is useful for the wide range of security and safety applications, a number of technologies have been pursued for human tracking. Computer vision has limited performance in poor visibility conditions, while the performance of infrared imagers can be temperature dependent. Human LADAR signatures may not highly discriminable from other moving clutter, and LADAR performance degrades in dusty and foggy conditions. UWB radar can provide a complementary technology for detecting and tracking humans, particularly in poor visibility or through-wall conditions, as it is little affected by dust and moisture. While this paper considers the problem of tracking humans based solely on UWB radar signals, UWB radar technology can profitably joined with other human tracking modalities to provide more robust tracking and detection in a wider variety of operating conditions.

Compared with RF, microwave, and mm-wave radar [1) 2)], UWB radar provides high-resolution ranging and localization due to the fine temporal resolution afforded by its wide signal bandwidth [3) 4) 5)]. However, the complex scattering behavior of UWB waveforms poses additional signal processing and tracking problems. In our previous work, Chang, et. al., developed an Expectation-Maximization Kalman Filter (EMKF) algorithm for UWB radar-based tracking of a fixed number of humans [6)]. However, because this prior work assumes a fixed number of targets, it is necessary to develop a Multi-Target Tracking (MTT) solution which allows for changing numbers of targets, false measurements (clutter), and missed detections (temporary occlusions).

An abundant MTT literature has considered military radar and computer vision tracking applications [7) 8) 9)]. However, the key differentiator of MTT for UWB radar-based tracking versus traditional applications is the multitude of observations (multipath scattering) per target in each scan, due to the short spatial extent of the transmitted UWB signal pulse width [10)]. Because the multi-path signals have a cluster like nature, a two-level data association problem: individual scatters must be properly associated with the correct clusters, and the clusters must be associated across radar scans to generate a consistent track of human movement. Wolf recently developed a Multiple-Hypothesis Tracking of Clusters (MHTC) algorithm for sorting and tracking extracellular neural recordings [11)], whose measurements arrive in an analogous cluster-like nature. We develop a variant of Wolf's algorithm for the UWB radar-based multi-human target tracking problem, which extends our previously developed algorithm to the more realistic case of varying target number. Recently, Lau, Arras, and Burgard [12)] have

also developed a related technique for multi-hypothesis tracking of groups of humans using LADAR. In addition to a focus on a different signal type, our method has a different decomposition of the probability densities needed to select the best joint clustering and track association hypotheses, as well as an explicit formula for computing the model evidence via a Laplacian approximation.

Section 2 presents the simple UWB radar multipath signal model that underlies our approach, and shows that waveform time-of-arrival can be interpreted as a point process governed by a Gamma probability distribution. Section 3 reviews our previous EMKF tracking algorithm for a fixed number of targets. Section 4 presents our proposed MHTC algorithm for tracking a variable number of humans, while Section 5 presents experimental results to illustrate and validate our approach.

2. UWB Signal Modeling

As compared with traditional narrow band radar, the wide bandwith of UWB radar (e.g. a 2 GHz bandwidth centered at 4GHz frequency in our experiments) allows for radar waveforms that are highly localized in time. A typical UWB waveform pulse, such as shown in **Fig. 1**, has a duration of ～0.5-1.5 ns. After the pulse is emitted, the scattered waveforms are recorded for a fixed interval of time. This interval establishes the effect range of the radar, and the data recorded during one interval is termed a "scan."

2.1 UWB Scattered Waveform Model

This paper considers a mono-static radar configuration where waveform pulses are transmitted from a single antenna and the scattered waveforms are received by a collocated antenna. An effective human detection and tracking strategy requires a model of UWB radar waveform propagation and interaction with the human body. A perfectly reflecting target, e.g. a metal plate with an infinite area, returns the impinging UWB electromagnetic wave along a single-path. However, for targets characterized by complex shapes whose spatial extent roughly equals the transmitted UWB signal pulse width, e.g. the human body, the returned UWB radar signal consists of multipath components [10], as the impinging UWB electromagnetic wave scatters independently from different human body parts at different times with various amplitudes (depending on the distance to the body part and the size, shape, and composition of the scattering part). Each of these different scattering pathways can be considered one component of the returned UWB radar signal. Thus, the returned UWB radar signal $w(t)$ can be approximated by a *specular multipath model* [13)14)]:

$$w(t) \approx \sum_j a_j p(t - n_j) \qquad (1)$$

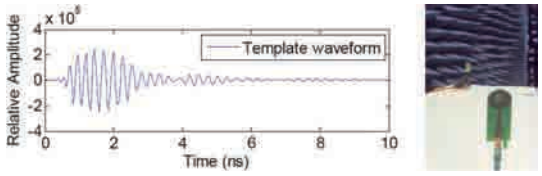

Fig. 1　Measured UWB waveform (left) and measurement setup

with a_j and n_j respectively representing the amplitude and time-of-arrival (TOA) of the j^{th} component of the received signal, and $p(t)$ is an elementary waveform shape, e.g., the transmitted radar waveform in free space. For example, the waveform is recorded over an interval $t \in [t_0, t_{\max}]$, which corresponds to a range of $r \in [r_0, r_{\max}] = [ct_0/2, ct_{\max}/2]$, where c is the speed of light (see details in [14)]). The specular multipath model is an approximation whose simplicity allows for real-time processing without compromising UWB radar's high time-resolution capability. Each path's TOA and amplitude can be estimated by the applying the CLEAN algorithm (with a given waveform template) to a scan [14) 15)].

CLEAN Algorithm Summary

1. Input :Waveform shape template $v(t)$; and detection threshold T_{clean} normalized at 1 meter.
2. Initialize : Form initial residual waveform $d_0(t) = w(t)$ for a scan. Set counter $i = 0$.
3. Signal Detection : Compute cross-correlation $r_{vd}(\tau)$ between $v(t)$ and $d_i(t)$; the time-index associated to the maximum magnitude of $r_{vd}(\tau)$ is the ith estimated TOA:

$$\hat{n}_i(t) = \arg\max_\tau \left| r_{vd}(\tau) \right|$$

The cross-correlation at $\hat{n}_i(t)$ is the i^{th} estimated amplitude:

$$\hat{a}_i(t) = r_{vd}(\hat{n}_i(t))$$

If $\hat{a}_i(t) < T_{clean}$, STOP.

4. Increment the iteration counter : $i \leftarrow i + 1$.

5. Residual waveform update:

$$d_i(t) = d_{i-1}(t) - \hat{a}_i(t)v(t - \hat{n}_i(t))$$

6. Iterate : Go to step 3.

Since UWB radar scatters from both stationary and moving objects, all scatters obtained from a complex test environment must be analyzed for human target candidates. To reduce the high computational cost associated to such analysis, a *moving target indication* (MTI) system, summarized in [14], is used to eliminate highly human-unlike scatters.

2.2 Human Scattered Waveform Characterization

In order to understand the basic scattering behavior, we constructed a database of UWB radar scans obtained while a human walked randomly in an open field within the vicinity of the radar (see details in [6]). The radar returns were calibrated and processed using the CLEAN algorithm to extract the amplitudes and TOAs of the scattering components. These returns were then manually segmented to ensure a correct data association between detected scatter paths and the human target. To characterize scattered waveforms from moving humans, we introduce two variables: human range and adjusted time-of-arrival. The human target's nominal range is defined as the first moment of the power range profile r [14]:

$$r = \frac{\sum_{j\in\Omega} a'^2 R_j}{\sum_{j\in\Omega} a'^2}$$

where $a' = a_j R_j^2$ is the j^{th} scattering path's amplitude normalized at 1 m (where the free space loss is compensated for the round-trip range), $R_j = [n_j \cdot c\ ]/2$ is the j^{th} scattering path's range[1], n_j is the TOA of the j^{th} scatter component, and is a set of path indices associated with the human target. It is convenient to introduce an adjusted TOA (ATOA) variable:

$$\delta_j(r) = R_j - r + K \qquad (3)$$

where r is the range to the human, and K is a constant offset related to the radar delay spread of a typical human.

Our studies have found that the ATOA histograms have a behavior consistent with a point process, thus he mono-static UWB radar scattering process for walking humans, under the specular multipath model in Equation (1), can be interpreted as *point process* governing the ATOAs. After studying common univariate distributions, we found that the ATOA histogram was best fit by a *Gamma distribution* whose mode lies at the human target location and whose probability density function (PDF) $f_\Gamma(\delta;\kappa;\theta)$ is:

$$f_\Gamma(\delta;\kappa;\theta) = \delta^{\kappa-1}\frac{\exp(-\delta/\theta)}{\theta^\kappa \Gamma(\kappa)} \quad \text{for} \quad \delta > 0 \qquad (4)$$

where $\Gamma(\cdot)$ is the Gamma function, and K, θ are respectively the Gamma distribution's *shape* and *scale* parameters[2]. In our application, the K parameter is a fixed value characteristic of humans, which is estimated from the database at K = 7.60 in **Fig. 2**. The θ parameter is related to target location, and is estimated during the tracking process. While our choice of the Gamma distribution was based on an empirical study, we note that the Gamma distribution exactly models the distribution of arrival times for Poisson distributed events. It is thus a plausible model for multi-path human scatter ATOAs.

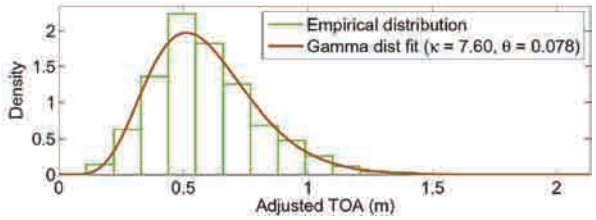

Fig. 2　Histgram of multi-path ATOA, with Gamma distribution fit.

3. Tracking a Fixed Number of Human Targets

For simplicity of exposition, this section summarizes our prior work [6], which forms the basis for the new developments of this paper. First we show how to track a fixed number of humans using an Expectation-Maximization Kalman Filter (EMKF) algorithm, where the expectation-maximization (EM) algorithm simultaneously associates individual scatter paths to each target and estimates each target's state. The next section, which represents the new contributions of this paper, shows how to add an MTT capability to this framework via the use of a cluster-based MHT procedure.

We define the state vector x of a human target as X =, [r v]^T where r and v respectively denote the range and velocity (time rate of change of the range) of the human target, and $(\cdot)^T$ denotes the transpose. For simplicity, we use a simple

random walk model to model human dynamics:

$$\mathbf{x}_{k+1} = \begin{bmatrix} 1 & \Delta T \\ 0 & 1 \end{bmatrix} \mathbf{x}_k + \begin{bmatrix} 0 \\ \omega \end{bmatrix} = A\mathbf{x}_k + B\omega$$

where ω is zero-mean white Gaussian noise with covariance q^2, B = [0　1]^T, $\Delta T = t_{k+1}$-t_k. The covariance of the process noise $B\omega$ is equal to Q = diag(0,q^2) . Note that our algorithm readily incorporates more complicated target dynamic models.

Based on the characterization of human UWB scatter as a point process, we model the multi-target multi-path scattering process as a *mixture model*, where each mixture component is a Gamma distribution associated with an individual human target. If there are G human targets in the observation environment, where G is known, the likelihood of the N TOA observations at time t_k, $Y^k = \{n_{j,k}\}_{j=1}^{N}$, is given by:

$$p\left(Y^k \mid \Theta^k\right) = \prod_{j=1}^{N} \sum_{g=1}^{G} \pi_k^g f_\Gamma\left(\delta_{l,k}\left(r_k^g\right); \kappa_k^g, \theta_k^g\right) \qquad (5)$$

where Θ_k is the set of model parameters at time t_k: $\Theta_k = \left\{\pi_k^g, r_k^g, \kappa_k^g, \theta_k^g\right\}_{g=1}^{G}$. Let $\hat{\mathbf{x}}_{k|l}^g$ and $P_{k|l}^g$ respectively denote the state estimate of the gth human target and its error covariance at time k, given measurements up to time l.

An Expectation Maximization Kalman Filter (EMKF) algorithm to update the G target state estimates from the radar scan obtained at time tk is given below. It unites a basic Kalman Filter (KF) state estimator with a data association process (implicitly carried out by the EM-algorithm) that associates individual multi-path returns to specific targets. The path-to-target association probability is modeled as the latent variable of the EM algorithm. Like any tracking algorithm, models for the uncertainties in the dynamic process and the measurements are required for effective tracking. The measurement error covariance used in the algorithm is the sum of a fixed term that describes the inherent noise in the radar processing circuitry, plus a data dependent term that fact that the measurement quality depends upon the number of multi-path returns obtained in a single scan (finite sample effect).

1. *Input* : TOAs $\{n_{j,k}\}_{j=1}^{N}$ of the G humans scatter paths at time k (calculated by applying the CLEAN algorithm to scan k).
2. *Initialize*: Initialize constant parameters: Gamma distribution parameter K (fixed for typical humans), offset K (see footnote 2), dynamic model transition matrix A, measurement matrix H = [1 0], process noise Q, the constant part of range measurement error covariance R_{fixed}, and iteration threshold T_{EM}. Initialize the mixture model parameters $\hat{\Theta}^{k,(0)}$ —typically the estimate from $t_k - 1$ serves as the starting point. Set counter $i = 0$.
3. *KF Dynamic propagation step* : Given the estimate $\hat{\mathbf{x}}_{k-1|k-1}^g$ with $P_{k-1|k-1}^g$ at time $k-1$, calculate the state estimate $\hat{\mathbf{x}}_{k|k-1}^g$ and its covariance $P_{k|k-1}^g$ at time k as

$$\begin{aligned} \hat{\mathbf{x}}_{k|k-1}^g &= A\hat{\mathbf{x}}_{k-1|k-1}^g \\ P_{k|k-1}^g &= AP_{k-1|k-1}^g A^T + Q \end{aligned} \qquad (6)$$

Set the initial estimate of the human range $\hat{r}_k^{g,(0)} = \hat{r}_{k-1}^{g,EM}$
4. *EM algorithm*: initialize the EM algorithm (steps 5 and 6) iteration counter, $i = 1$.
5. *EM E-step* : Using the current i^{th} iteration parameter estimates $\hat{\Theta}^{k,(i)}$ and measurements Y , compute the conditional expectation $\hat{z}_{jg}^{(i+1)} = E\left[z_{jg} \mid n_{j,k}, \hat{\Theta}^{k,(i)}\right] \in [0,1]$ as

$$\hat{z}_{jg}^{(i+1)} = \frac{\pi_k^g f_\Gamma\left(\delta_{j,k}^{g,(i)}; \kappa, \hat{\theta}_k^{g,(i)}\right)}{\sum_{n=1}^{G} \pi_k^n f_\Gamma\left(\delta_{j,k}^{n,(i)}; \kappa, \hat{\theta}_k^{n,(i)}\right)},$$

where $\hat{z}_{jg}$ is the probability that multi-path component j is generated by target g-i.e., the TOA observation to target range measurement association probability. The ATOAs are calculated by the current ith iteration human range estimate as $\delta_{j,k}^{g,(i)} = cn_{j,k}/2 - \hat{r}_k^{g,(i)} + K$
6. *EM M-step* : Given $\hat{z}_{jg}^{(i+1)}$, find the parameter estimates $\hat{\Theta}^{k,(i)}$ that maximizes the complete-data log-likelihood function:

$$l_{CD}\left(\Theta^k \mid Y^k, Z\right) = \sum_{j=1}^{N} \sum_{g=1}^{G} z_{jg} \log\left[\pi_k^g f_\Gamma\left(\delta_{j,k}^g; \kappa; \theta_k^g\right)\right] \qquad (7)$$

which models the probability, given the set of all data association assignments Z = {z_{jg}}, that the multi-path range measurements are generated by G targets located at positions parameterized by Θ^k . Using the Lagrange multiplier method with the constraint of $\pi_k^g \geq 0$ and $\sum_{g=1}^{G} \pi_k^g = 1$, one obtains the following estimates of π_k^g and θ_k^g :

$$\hat{\pi}_k^{g,(i+1)} = \frac{\sum_{j=1}^{N} \hat{z}_{jg}^{(i+1)}}{N} \quad \text{and} \quad \hat{\theta}_k^{g,(i+1)} = \frac{\sum_{j=1}^{N} \hat{z}_{jg}^{(i+1)} \delta_{j,k}^{g,(i)}}{\kappa \sum_{j=1}^{N} \hat{z}_{jg}^{(i+1)}}$$

The range estimate at the mode of the distribution is:

$$\hat{r}_k^{g,(i+1)} = (\kappa - 1)\hat{\theta}_k^{g,(i+1)} + \hat{r}_k^{g,(i)} - K$$

7. *Iteration criterion* : If $\sum_{g=1}^{G} \left| \hat{r}_k^{g,(i+1)} - \hat{r}_k^{g,(i)} \right| > T_{EM}$, go to step 5 with $i \leftarrow i+1$. Otherwise, each TOA $n_{j,k}$ is assigned to the g^{*th} human via $g^* = \text{argmax}\, \hat{z}_{j,g}$. Set the estimate of human range $\hat{r}_k^{g,EM} = \hat{r}_k^{g,(i+1)}$, and the estimation error variance $R_k = R_{fjx} + [(\kappa - 1)\hat{\theta}_k^{g,(i+1)}]^2 / \kappa N$
8. *Measurement Update* : Set the human range measurement $y_k^g = \hat{r}_k^{g,EM}$ Update the Kalman gain K_k^g , the a posterior state estimate $\hat{\mathbf{x}}_{k|k}^g$, and the error covariance $P_{k|k}^g$ as

$$\begin{aligned} K_k^g &= P_{k|k-1}^g H^T \left(H P_{k|k-1}^g H^T + R_k \right)^{-1} \\ \hat{\mathbf{x}}_{k|k}^g &= \hat{\mathbf{x}}_{k|k-1}^g + K_k^g \left(y_k^g - H \hat{\mathbf{x}}_{k|k-1}^g \right) \\ P_{k|k}^g &= \left(I - K_k^g H \right) P_{k|k-1}^g \end{aligned} \tag{8}$$

Experimental validation of this method for the case of a fixed number of humans can be found in [6].

4. Tracking a Variable Number of Human Targets

In a realistic environment, the number of human targets will vary with time, as targets may go in and/or out of the observation volume. Additionally, the tracking system should also be able to handle clutter (e.g. non-human objects and false measurements) and missed detections (temporary occlusions), allowing for an appropriate segmentation process, simultaneously. The algorithm summarized above also has no inherent mechanism to construct consistent tracks across multiple scans. Thus, it is necessary to develop a Multi-Target-Tracking (MTT) solution for these practical realities. The MTT technique should solve two types of data association problems: (1) all multipath scatter components must first be segregated according to their generating source (the observation–measurement association problem or the multipath scatter–cluster association problem); and then each scattering cluster must be associated to clusters from previous scans, thus tracking the UWB scattering response of putative human targets (the measurement–target or track assignment association problem). This differes from the standard MHT problem which only focuses on the single track assignment data association problem.

We propose to use an Multi-Hypothesis-Testing (MHT) approach which maintains many possible data association hypotheses and propagates the corresponding target state estimates for each hypothesis, implicitly deferring decisions if necessary in anticipation that subsequent data measurements will resolve any ambiguity [16]. However, unlike traditional MHT in military radar and computer vision tracking applications [8) 9)], this problem has the additional complexity that targets are only observed indirectly via clusters of scattering path measurements. To incorporate this additional complexity, we adapt a recently developed MHTC method [11] that was originally developed for dynamic sorting and tracking of neural signals. This algorithm propagates various possibilities for how to assign measurements to clusters and then clusters to existing target tracks. It uses a delayed decision-making logic to resolve data association or track association ambiguities. It also maintains several options, termed model hypotheses, for how to cluster the observations of each interval. This combination of clustering nd tracking in a single solution enables MHTC to robustly maintain the identities of cluster-producing targets.

4.1 MHTC Framework

The framework summarized in the previous section must be extended in several directions to allow for robust tracking of variable numbers of humans in cluttered environments. Section 4.1.1 introduces the more complex types of hypotheses which must be considered to solve the MTT-MHT problem of UWB-radar tracking of humans. This section also defines the overall hypothesis probabilities that must be calculated during the tracking process. In essence, the ensuing sections expand the composite hypothesis probability into its components. Section 4.2 shows how to properly use the clustering/tracking results of scan k－1 as a Bayesian prior for the processing of scan k. Section 4.3 briefly summarizes the hypothesis tree structure that incorporates both data association hypotheses across scans and various clustering hypotheses within scans. Section 4.4 then summarizes the MHTC algorithm, while Section 4.5 integrates all of the technical developments of this section to define the global hypothesis probability that is at the heart of the tracking algorithm.

4.1.1 Hypothesis Terminology

We define two types of hypotheses in MHTC. A model hypothesis represents a possible clustering of the multipath observations, and is denoted by M_m. Different models account for differing numbers of humans, where the number of humans is denoted by G_m. The l^{th} data association or track association hypotheses, $h_l = \{\tau_l, \nu_l, \phi_l\}$, l=1,*K*,*L*, assigns each cluster in a given model hypothesis to a target or track (or marks it as spurious)[4]: The set contains the assignments of the model's clusters to known targets, $\tau_l = \{(g_1, j_1), \quad, (g_{N_\tau}, j_{N_\tau})\}$, where each indexed pair (g, j) matches the g^{th} cluster to the j^{th} human target; $\nu_l = \{g_1, \quad, g_{N_\nu}\}$ indexes the model's clusters that are identified as new human targets; and $\phi_l = \{g_1, \quad, g_{N_\phi}\}$ holds the indices of false clusters (spurious groupings of outliers, clutter, or similar clustering errors) in the current model. Note that N_τ , N_ν, , and N_ϕ are the respective cardinalities of these sets, and a legal hypothesis must assign every measurement (a clustering of the data) to only a single target (or classify it as false) and may only assign at most one measurement to each target so that the total number of measurements is $G_m = N_\tau + N_\nu + N_\phi$.

We call the combination of a data association hypothesis and its parent model hypothesis a particular *joint hypothesis* at time k, $H_l^k = \{M_{m(l)}, h_l\}$. The joint hypothesis H_l^k thus postulates a complete set of data associations for time k, including the multipath TOA-to-cluster (observation-to-measurement) associations in $M_{m(l)}$ and the cluster-to-human (measurement-to-target) associations in h_l. A particular joint hypothesis is combined with its *parent hypothes* is $H_{\rho(l)}^{1:k-1}$ at time $k-1$ (we consider M model classes for each parent hypothesis) to define a *global hypothesis*, $H_l^{1:k} = \{H_l^k, H_{\rho(l)}^{1:k-1}\}$, which includes the full history of all model and data association hypotheses from time 1 through k. Finally, it is convenient to define Ω^k as the set of all L surviving global hypotheses $\{H_l^{1:k}\}_{l=1}^L$ and all data $Y^{1:k}$ from time 1 through k, which thus provides all relevant measured and hypothesized information at time k: $\Omega_k = \left\{\left\{H_l^{1:k}\right\}_{l=1}^L, Y^{1:k}\right\}$

4.1.2 Probability Models

Given a set of targets tracked in the parent hypothes is $H_{\rho(l)}^{1:k-1}$, the probabilities of the existence of tracked targets and appearance of new measurements in radar scan at time k must be modeled. For simplicity, let us assume that the probability that the j^{th} existing target is detected (i.e., produces a multi-path cluster) is considered a Bernoulli trial with probability $P_{d,j}$. If the target is detected, the associated range measurement r_k^g is expected to appear near the target's predicted location with a Gaussian distribution,

$$p\left(r_k^g \mid (g,j) \in \tau_l, h_l, H_{\rho(l)}^{1:k-1}, Y^{1:k-1}\right) = f_N\left(r_k^g \mid \hat{r}_{k|k-1}^j, S_k^j\right)$$
$$= \frac{1}{\sqrt{2\pi S_k^j}} \exp\left\{-\frac{\left(r_k^g - \hat{r}_{k|k-1}^g\right)^2}{S_k^j}\right\}$$

where the Gaussian PDF is denoted by f_N, the mean and covariance are the predicted measurement $\hat{r}_{k|k-1}^j \in \mathbf{x}_{k|k-1}^j$ and the innovation covariance $S_k^j = HP_{k|k-1}^j H^T + R_k$, respectively, provided by the dynamic update equations (6) of the Kalman filter.

The numbers of new targets or false clusters appearingin a given time interval are each modeled by a Poisson distribution with respective rates λ_ν and λ_ϕ. If a measurement originates from a new target or false cluster, it may arise anywhere in the observation volume V with a uniform PDF:

$$p(r_k^g \mid g \in \{\nu_l, \phi_l\}, h_l, H_{\rho(l)}^{1:k-1}, Y^{1:k-1}) = 1/V$$

The parameters $P_{d,j}$, λ_ν, and λ_ϕ are set by the user and may vary across scanning intervals. Experiments indicate that the precise values are not required for effective operation of the algorithm.

4.2 MAP Clustering for Human Tracking

In order to improve clustering and tracking, we convert the EM algorithm to a Maximum A-Posteriori (MAP) optimization rather than an Maximum Likelihood (ML) optimization of the Gamma mixture model proposed in previous sections. The MAP method uses information from the preceding scans as a prior to bias the propbabilities of the joint hypothesis in the current scan, while still admitting changes in the number of human targets. Using Bayes' rule, the MAP parameter estimates can be derived as

$$p(\Theta_m^k \mid Y^{1:k}, M_m) \propto p(Y^k \mid \Theta_m^k, M_m) p(\Theta_m^k \mid Y^{1:k-1}, M_m) \quad (10)$$

where Θ_m^k represents the mixture model parameters at time step k, for a given model M_m. In Eq. (10), the first term represents the likelihood of the current observation Y^k given parameter estimates, and the second term represents a prior probability which provides the parameter distribution based on previous observations.

4.2.1 Likelihood and Prior terms

In the likelihood term of Eq. (10), an outlier distribution (defined as a uniform distribution with magnitude 1/V over the observation volume) as added to the *G*m Gamma mixture components in Eq. (5) in order to capture false positives of detected TOAs. Hence, the mixture likelihood term can be represented as

$$p(Y^k \mid \Theta_m^k, M_m) = \prod_{j=1}^{N}\left[\pi_k^0 \frac{1}{V} + \sum_{g=1}^{G_m} \pi_k^g f_\Gamma(\delta_{j,k}^g; \kappa, \theta_k^g)\right] \quad (11)$$

where $\pi_k^0 = 1 - \sum_{g=1}^{G_m} \pi_k^g$

since the mixture weights must sum to unity. After incorporating the observation-to-measurement association indicator Z, the complete data log-likelihood is a modified form of Eq. (7):

$$l_{CD}(\Theta_m^k \mid Y^k, Z, M_m) = \sum_{j=1}^{N}\left[z_{j0} \log\left[\pi_k^0 \frac{1}{V}\right] + \sum_{g=1}^{G_m} z_{jg} \log\left[\pi_k^g f_\Gamma\left(\delta_{j,k}^g; \kappa, \theta_k^g\right)\right]\right] \quad (12)$$

Next, in the prior term, the model parameters are assumed to be independent across mixture components and across each parameter; hence,

$$p(\Theta_m^k \mid Y^{1:k-1}, M_m) = C\prod_{g=1}^{G_m} p(r_k^g \mid Y^{1:k-1}, M_m) \quad (13)$$

where the diffuse priors on the parameters θ_k^g and π_k^g,

$$C = \prod_{g=1}^{G_m} p\left(\theta_k^g \mid Y^{1:k-1}, M_m\right) \cdot p\left(\pi_k^g \mid Y^{1:k-1}, M_m\right)$$

, are given as a constant, since the parameters are are less informative model elements than the range of each cluster r_k^g in practical human clustering and tracking consistency. To establish priors on the cluster range, the g^{th} cluster range r_k^g in time k is sought near to any of the cluster ranges found in time $k-1$, and thus a Gaussian mixture (based on Eq. (9)) involving all of the cluster ranges at t_k-1 is used as a prior. To allow for the possibility that the gth cluster represents a new human that was not observed in scan $k-1$, a uniform distribution component defined over the observation volume V is included as well. Hence, Incorporating Eq. (9) into (13), the complete prior on the mixture parameters is

$$p\left(\Theta_m^k \mid Y^{1:k-1}, M_m\right) \quad (14)$$

$$= C\prod_{g=1}^{G_m}\left[\frac{w_k^0}{V} + \sum_{j=1}^{\hat{G}^{k-1}} w_k^j f_N\left(r_k^g \mid \hat{r}_{k|k-1}^j, S_k^j\right)\right] \quad (15)$$

where the mixture weight w_k^j is defined as

$$w_k^j = \begin{cases} (1/c)\lambda_0 & j = 0 \\ (1/c)P_{d,j} & j = 0, \mathrm{K}, \hat{G}^{k-1} \end{cases}$$

where $\lambda 0 = \lambda_v + \lambda_\phi$ is the combined expected number of newly appearing humans and the false clusters in a scan.

4.2.2 Extending EM to Account for Cluster Location Priors

Note that the prior term in Eq. (14) resembles the mixture likelihood term in Eq. (11), and would in fact share the same difficulty of providing closed-form solution for the optimal parameters. Similarly, the EM algorithm can be applied by introducing a set of cluster association indicators Z = $\{\zeta_{g,j}\}$ that indicates cluster membership to a particular human target,

$$\zeta_{gj} = \begin{cases} 1 & \text{if cluster } C_g \text{ at scan } k \text{ is associated} \\ & \text{with human target } j \text{ at scan } k-1 \\ 0 & \text{otherwise} \end{cases}$$

Employing the classical complete-data approach, the cluster association indicators and the mixture prior defined term in Eq. (14) determine the complete-data log prior on the mixture parameters:

$$\log p\left(\Theta_m^k, Z \mid Y^{1:k-1}, M_m\right) = \sum_{g=1}^{G_m}\left\{\zeta_{g0} \log\left[\frac{w_k^0}{V}\right] + \sum_{j=1}^{\hat{G}^{k-1}} \zeta_{gj} \log\left[w_k^j f_N\left(r_k^g \mid \hat{r}_{k|k-1}^j, S_k^j\right)\right]\right\} + \log C \quad (16)$$

Rewriting Eq. (10) to include the TOA membership indicators Z as well as the cluster association indicators Z gives the complete-data posterior,

$$p\left(\Theta_m^k, Z \mid Y^{1:k}, Z, M_m\right) \propto p\left(Y^k, Z \mid \Theta_m^k, Z, M_m\right) \cdot p\left(\Theta_m^k, Z \mid Y^{1:k-1}, M_m\right) \quad (17)$$

As it is convenient to work with the log-posterior, take the logarithm of Eq. (17) and substitute in Eq. (12) and (16),

$$\begin{aligned} &\log p\left(\Theta_m^k, Z \mid Y^{1:k}, Z, M_m\right) \\ &= \sum_{j=1}^{N}\left\{z_{j0} \log\left[\pi_k^0 \frac{1}{V}\right] + \sum_{g=1}^{G_m} z_{jg} \log\left[\pi_k^g f_\Gamma\left(\delta_{j,k}^g\left(r_k^g\right); \kappa, \theta_k^g\right)\right]\right\} \\ &+ \sum_{g=1}^{G_m}\left\{\zeta_{g0} \log\left[\frac{w_k^0}{V}\right] + \sum_{j'=1}^{\hat{G}^{k-1}} \zeta_{gj'} \log\left[w_k^{j'} f_N\left(r_k^g \mid r_{k|k-1}^{j'}, S_k^{j'}\right)\right]\right\} + \log C \end{aligned} \quad (18)$$

This complete-data log-posterior is the object equation of

the EM algorithm's iterations, which follow.

E-Step : As in the classical EM algorithm, given the parameter estimates from the M-step, the expectation of each TOA membership indicator, $\hat{z}_{i,g}$ is:

$$\hat{z}_{ig}=\begin{cases}\dfrac{\hat{\pi}_k^0(1/V)}{\hat{\pi}_k^0(1/V)+\sum_{n=1}^{G_m}\hat{\pi}_k^n f_T\left(\delta_{j,k}^n(\hat{r}_k^n);\kappa,\hat{\theta}_k^n\right)} & g=0\\ \dfrac{\hat{\pi}_k^g f_T\left(\delta_{j,k}^g(\hat{r}_k^g);\kappa,\hat{\theta}_k^g\right)}{\hat{\pi}_k^0(1/V)+\sum_{n=1}^{G_m}\hat{\pi}_k^n f_T\left(\delta_{j,k}^n(\hat{r}_k^n);\kappa,\hat{\theta}_k^n\right)} & g=1,\mathrm{K},G_m\end{cases}$$

The expectation of the cluster association indicators, i.e., $\hat{\zeta}_{g,j}=\mathrm{E}\left[\zeta_{g,j}\,|\,Y^{1:k},\hat{\Theta}_m^k\right]$, has an analogous form:

$$\hat{\zeta}_{gj}=\begin{cases}\dfrac{w_k^0/V}{(w_k^0/V)+\sum_{l=1}^{\hat{G}^{k-1}}w_k^l f_T(\hat{r}_k^g\,|\,\hat{r}_{k|k-1}^l,S_k^l)} & j=0\\ \dfrac{w_k^l f_T(\hat{r}_k^g\,|\,\hat{r}_{k|k-1}^l,S_k^l)}{(w_k^0/V)+\sum_{l=1}^{\hat{G}^{k-1}}w_k^l f_T(\hat{r}_k^g\,|\,\hat{r}_{k|k-1}^l,S_k^l)} & j=1,\mathrm{K},\hat{G}^{k-1}\end{cases}$$

M-Step : using the Lagrange multiplier method with the constraints of $\sum_{g=0}^{G_m}\pi_k^g=1$ and $\sum_{j=0}^{\hat{G}^{k-1}}w_k^j=1$, one obtains the following estimates of π_k^g, and θ_k^g :

$$\hat{\pi}_k^g=\frac{\sum_{j=1}^N\hat{z}_{jg}}{N}\quad\text{and}\quad\hat{\theta}_k^g=\frac{\sum_{j=1}^N\hat{z}_{jg}\delta_{j,k}^g}{\kappa\sum_{j=1}^N\hat{z}_{jg}}\qquad(19)$$

where the estimates remain the same as the classical ML clustering version in Section 3, since the prior term in Eq. (18) is independent of the parameters π_k^g and θ_k^g. However, the estimate of r_k^g does not have a closed form formula due to the ATOA's dependency on the cluster range as in Eq. (3), as well as the scale parameter θ_k^g dependency on the cluster range as in Eq. (19) followed by Eq. (3). However, a numerical solution can be provided by using Newton's method as

$$\hat{r}_k^{g,(i+1)}=\hat{r}_k^{g,(i)}-\frac{A}{B}\qquad(20)$$

where

$$A=\sum_{j=1}^N\hat{z}_{jg}\left[\frac{1}{\hat{\theta}_k^g}-\frac{\kappa-1}{\delta_{j,k}^g}\right]-\sum_{j'=1}^{\hat{G}^{k-1}}\hat{\zeta}_{gj'}\frac{\hat{r}_k^{g,(i)}-\hat{r}_{k|k-1}^{j'}}{S_k^{j'}}$$

$$B=\sum_{j=1}^N\hat{z}_{jg}\left[\frac{1}{\kappa(\hat{\theta}_k^g)^2}-\frac{\kappa-1}{(\delta_{j,k}^g)^2}\right]-\sum_{j'=1}^{\hat{G}^{k-1}}\frac{\zeta_{gj'}}{S_k^{j'}}$$

4.3 Hypothesis Tree Structure

As shown in **Fig. 3**, the MHTC algorithm extends the traditional MHT hypothesis tree to include model hypotheses as well as data association hypotheses: to each parent node from t_k-1 there are multiple model hypotheses describing various ways that the data in scan k can be clustered, and each of these hypotheses has various children hypotheses about how the clusters in scan k can be associated to target tracks in scan $k-1$. If L global hypotheses exist/survive at time $(k-1)$ and we consider $\bar{M}$ model classes spawned for each of L parent hypotheses, then $(L\bar{M})$ model hypotheses are formed at time k, each of which is optimized according to the MAP EM procedure of Section 4.2. By use of Murty's algorithm [17], only the L best data association hypotheses are retained at time k from $(L\bar{M})$ data association hypotheses, succeeded by the $(L\bar{M})$ model hypotheses.

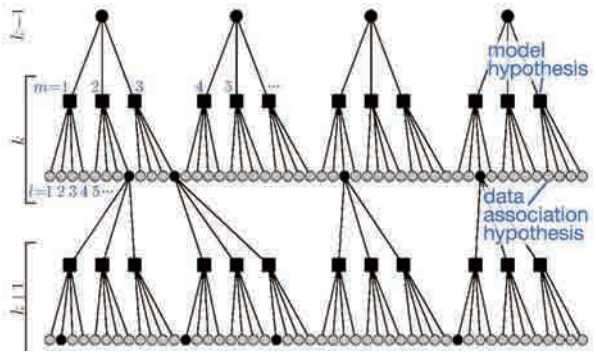

Fig. 3　MHTC hypothesis tree structure, illustrating the integration of model hypotheses into the traditional MHT framework, using L = 4 and $\bar{M}$ = 3. Squares represent model hypotheses (i.e., clustering output) and black circles represent surviving data association hypotheses at each time step.

4.4 Overview of the MHTC Process

This section integrates the technical developments of the previous sections to summarizes the MHTC process of combined clustering and multiple hypothesis tracking.

Step 1. Initialize the EM and Gamma mixture model parameters (see the initialization of the EMKF algorithm in Section 3).

Step 2. Given $k-1$ and the measurement update from time $k-1$ (see Step 8), for each parent hypothesis predict the target states (and their covariances) using the Kalman Filter dynamic update equations in Eq. (6).

Step 3. For every parent hypothesis in $k-1$, a set of candidate mixture model classes $\{M_m\}$ are postulated, which will be used to cluster the current data $Y^k=\{n_{j,k}\}_{j=1}^N$, pre-

processed by the MTI system and the CLEAN algorithm. A diversity of model classes are required primarily because the number of clusters G_m is unknown, so that various model orders are attempted and each resulting model hypothesis is analyzed. To save computation in very unlikely model classes, one can calculate the probability of a model class and test it against a threshold β:

$$P\left(M_m \mid H_{\rho(m)}^{1:k-1}, Y^{1:k-1}\right) > \beta \tag{21}$$

An expression for this probability, which depends on the probabilities of target detection, new targets, and false clusters, is provided in **Table 1**. Model classes that do not pass this thresholding test are discarded.

Step 4. For each model class, optimize the assignment of scattering multi-paths to individual model clusters, and optimize the cluster parameters using the MAP EM algorithm of Section 4.2.2. Note, to carry out this step, each model requires a set of "seed" clusters. The seed clusters are generated by starting with the clustering solution of the previous step, and then by adding or removing clusters according to the different hypotheses associated with each model. For example, new seeds are placed at the sensing boundaries to account for incoming targets; previous clusters are "split" into two clusters to allow for possible misclustering in the previous step; random seeds are added to account for spurious clusters, etc. (see [11] for more details).

Step 5. The evidence of each model hypothesis is calculated as $p\left(Y^k \mid M_m, H_{\rho(m)}^{1:k-1}, Y^{1:k-1}\right)$, possibly using the Laplace'smethod [19]. For computational savings, one could prune highly unlikely models as above.

Step 6. The core step in MHT generates the data association hypotheses, $h_l = \{\tau_l, \nu_l, \phi_l\}$. Murty's *L*-best ranked linear assignment algorithm is used to produce only the *L* best data association hypotheses from each parent cluster hypothesis, obviating the need for full enumeration of all possible data associations.

Step 7. Suppose that a total of ~M model hypotheses exist at this time, each of which has now spawned L data association hypotheses. From the (*ML*) hypotheses that have been generated, the most probable L global hypotheses (consisting of a joint model and data association hypothesis) are selected. Evaluating each model and data association hypothesis together with its parent hypothes is $H_{\rho(l)}^{1:k-1}$, the probability of each new global hypothesis $P(H_l^{1:k} \mid Y^{1:k})$ can be calculated, as detailed in Section 4.5. This step provides the set of *L*-best global hypotheses in Ω^k.

Step 8. Finally, for each $H_l^{1:k} \in \Omega^k$, the hypothesized data associations hl, along with the optimized parameters Θ_m^k of the corresponding model hypothesis, are used to update the Kalman Filter measurement update equations in Eq. (8).

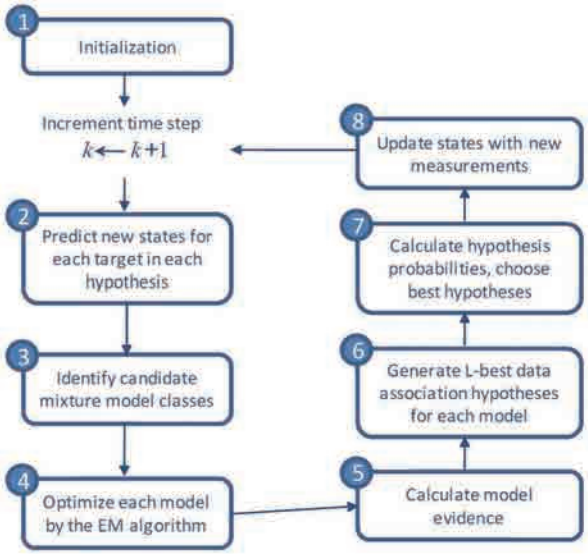

Fig. 4　MHTC process diagram. See text for description of each step. Steps 1-8 indicate core clustering and hypothesis tracking procedures

4.5　MHTC Probabilities

The final hypothesis selection of the MHTC algorithm for scan k is based on the global hypothesis given all collected data, $P(H_l^{1:k} \mid Y^{1:k})$. The expression for this probability includes all relevant measures about the parent hypothesis, model hypothesis, and data association hypothesis. This *global hypothesis probability* may be expressed as

$$P\left(H_l^{1:k} \mid Y^{1:k}\right) \approx \frac{1}{C} \frac{\mathcal{P}_{1,l}\,\mathcal{P}_{2,l}}{\sum_{n\in\Gamma} \mathcal{P}_{1,n}\,\mathcal{P}_{2,n}} \mathcal{P}_3\,\mathcal{P}_4\,\mathcal{P}_5 \tag{22}$$

where *C* is a normalization constant, Γ is the set of indices of all legal data association hypotheses given the model hypothesis $M_m(l)$. The factors (P1,l, P2,l, etc.) have natural interpretations for why they influence the global hypothesis probability and are described in **Table 1**. The proof for Eq.(22), which entails a combination of Bayes'Rule, the chain rule, and the Laplace's method for approximating integrals, may be found in [11], along with a derivation for the expressions in **Table 1**.

To calculate L-best data association hypotheses $\{h_l\}$ from each model hypothesis M_m in Step 6 of the MHTC algo-

rithm, only the product ($\rho_{1,l}, \rho_{2,l}$ etc.) needs to be examined, as all other factors in (22) are identical for a given model hypothesis. Thus, we refer to this product as the data association hypothesis plausibility. To formulate the data association problem such that Murty's algorithm may be applied, we construct a cost matrix for the corresponding linear assignment problem of mapping current measurements to known targets (including the notions of new targets and false clusters), where the total cost of an assignment hypothesis is equivalent to using (P1,l P2,l). See [11] for details.

5. Experimental Results

5.1 Experimental Setup

To test the MHTC algorithm, UWB mono-static radar measurements were conducted for time-varying number of human targets walking in and out of the radar observation volume of a Time Domain Puls On 210 monostatic UWB radar. As a ground truth to evaluate the radar tracking performance, two LADARs (SICK AG short range LIDAR) were placed facing each other to sense the observation volume, simultaneously, with the scanning azimuth angle in the range [0◦, 180◦] and with a scanning frequency of 75 Hz. As shown in **Fig. 5**, LADAR1 was placed coaxially above the radar,while LADAR2 was placed at 8.915 m away from LADAR1 along the longitudinal axis through LADAR1. The height of the radar was 0.483 m (around knee level), and the height of LADAR1, and LADAR2 was 1.321mand 1.118m (around chest level), respectively. The locations and orientations of the radar and both LADARs were calibrated using a procedure similar to the calibration method in [6]. The experiment was also recorded on video with a rate of 30 frames/sec. The radar range was set at 0 m to 9.087 m. The radar scanning period ΔT was 0.0787 sec/scan = $(12.7 \text{ scans/sec})^{-1}$, and the waveform sampling resolution was 41.33 ps with the range resolution of 0.0062 m. Time synchronization between the LADARs was automated, since both were connected to the same computer. Synchronization between the radar and LADARs was aided by the use of a predetermined and distinctive motion of the first human to enter the common sensing range. To test the 1-dimensional tracking performance for a single transmitting and a single receiving antenna radar system, the humans under test were instructed to walk in predetermined sectors so that no occlusion would occur.

Fig. 6(a) shows 572 unprocessed scans (each column represents the magnitude of a single scanned waveform over the sensing range, where the waveform magnitude is scaled from 0 in black to 3000 in white. Magnitudes over 3000 are clipped to 3000). Moving human targets' trajectories can be seen in **Fig. 6(a)**, while the horizontal patterns in the near range (< 2.2 m) represent direct antenna coupling effects from the transmitting antenna direct to the receiving antenna. The horizontal patterns in the far range around 8.8 m represent the scatters fromthe LADAR2 supporting structure. During the interval from scan 150 to 200, the LADAR2 supporting structure was on the blocked line-of-sight by a standing human so that the scatters from the structure were not observed distinctly. **Fig. 6(b)** shows a video image, LADAR range measurements, and the measured UWB radar scan 493 of two walking humans, as recorded by synchronized video camera, two LADARs, and a monostatic UWB radar, respectively. In the radar scan, scattering patterns of two humans are shown around at the ranges of 3.5m and 4.5 m, where the LADAR range measurements are observed at the corresponding ranges. It is noted that the LADAR measurements for the human at 4.5 m far shows an elliptical shape of the human's chest level cross section by using two LADARs. In the radar scan, direct antenna coupling effects and the scatters fromthe LADAR2 supporting structure were sensed at near range (< 2.2 m) and far range (～8.8m), respectively.

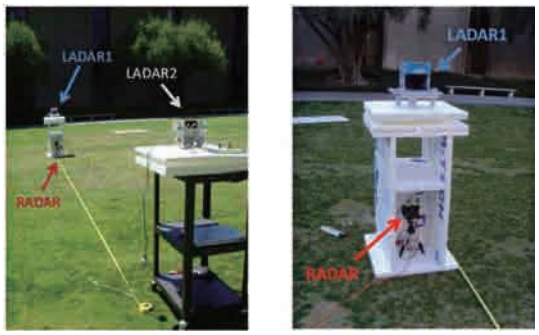

Fig. 5　Experimental setup picture.

Table1　Factors in Global Hypothesis Probability

	Definition	Expression for Model in Equation (22)	Interpretation
$\mathcal{P}_{1,l}$	$p\left(\{\hat{r}_k^g\}_{g=1}^{G_{m(l)}} \mid H_l^{1:k}, Y^{1:k-1}, \hat{\Theta}_{m(l)}^k\right)$	$\left[\prod_{(g,j)\in\tau_l} f_{\mathcal{N}}\left(\hat{r}_k^g \mid \hat{r}_{k\mid k-1}^j, S_k^j\right)\right]\left[\prod_{g\in\nu_l}\frac{1}{V}\right]\left[\prod_{g\in\phi_l}\frac{1}{V}\right]$	ranges' likelihood under h_l
$\mathcal{P}_{2,l}$	$p\left(H_l^k \mid H_{\rho(l)}^{1:k-1}, Y^{1:k-1}\right)$	$A_m\left[\prod_{j=1}^{J} f_{\mathcal{B}}\left(\delta_{j,l}\mid \mathrm{P}_{\mathrm{d},j}\right)\right](\lambda_\nu)^{N_\nu}(\lambda_\phi)^{N_\phi}$	joint hypothesis prior [a]
$\mathcal{P}_3$	$P\left(\mathcal{M}_{m(l)} \mid H_{\rho(l)}^{1:k-1}, Y^{1:k-1}\right)$	$\sum_{N_\tau=0}^{J}\left[\frac{(\lambda_0)^{G_m-N_\tau}e^{-\lambda_0}}{(G_m-N_\tau)!}\sum_{\delta\in\Upsilon}\prod_{j=1}^{J} f_{\mathcal{B}}\left(\delta_{j,l}\mid \mathrm{P}_{\mathrm{d},j}\right)\right]$	model hypothesis prior [b]
$\mathcal{P}_4$	$p\left(Y^k \mid \mathcal{M}_{m(l)}, H_{\rho(l)}^{1:k-1}, Y^{1:k-1}\right)$	see [18] for the Laplace's method (or other approximation)	model evidence
$\mathcal{P}_5$	$P\left(H_{\rho(l)}^{1:k-1} \mid Y^{1:k-1}\right)$	same as Eq. (22), from previous time step	parent hypothesis probability

[a] A_m is a constant depending on the model class and does not require calculation. $f_{\mathcal{B}}$ is the Bernoulli distribution, and $\delta_{j,l}$ is an indicator variable of whether the j^{th} target is tracked under the l^{th} hypothesis ($j \in \tau_l$).

[b] J is the number of existing targets, $\boldsymbol{\delta}$ is a vector of indicator variables δ_j, $j = 1, \ldots, J$, and Υ is the set of all possible $\boldsymbol{\delta}$ for a given J.

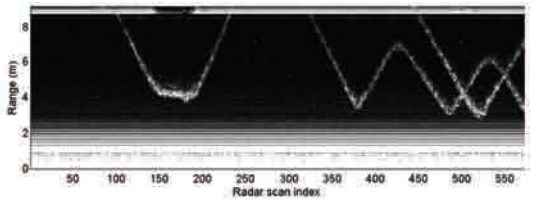

Fig. 6(a) Representation of 572 unprocessed radar scans.

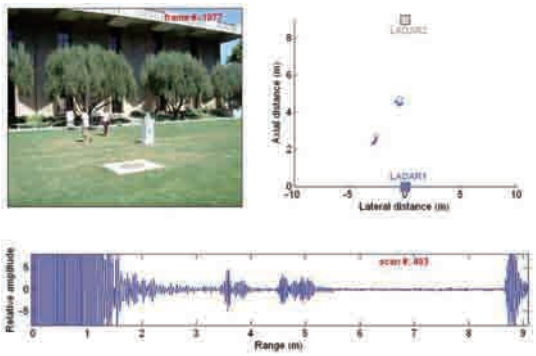

Fig. 6(b) Scattered UWB waveform for scan 493 (bottom), a synchronized video image (left-top), and synchronized two LADAR range measurements (right-top) for two walking humans.

Fig. 6 Measured data for the MHTC algorithm test

5.2 Results on the MHTC algorithm

To apply the MHTC algorithm to the radar measurements in Section 5.1, the EM and Gamma mixture model parameters were initialized as $\kappa = 7.60$, $K = 0.533$ m, $P_{dj} = 0.98$, $\lambda_v = 0.01$, $\lambda_\phi = 0.0105$, $\beta = 0.7$, and $L = 6$. The radar measurements were processed by the MTI system to eliminate antenna coupling effects and static background scatters, and processed by the CLEAN algorithm to estimate the amplitudes and TOAs (or range) of the scattering multipath components, as an example for scan 493 is shown in **Fig. 7(a)**. **Fig. 7(b)** shows theMAP EMclustering results for given two seeds from the a priori estimates of ranges in the KF ($\hat{r}_{493|492}^{A}$ =3.4734 m and $\hat{r}_{493|492}^{B}$ =4.8518 m)[7]. The resolved 7 TOA observations were associated with 2 (hypothetical) clusters to construct a Gamma mixture model so that their range (at the mode of each Gamma distribution) was computed to be so that two clusters' ranges (or range measurements) of each cluster were provided as r_{493}^{1} = 3.6868m and r_{493}^{2} = 4.8337 m at the mode of each Gamma mixture component[8]. Note that different number and/or range of seeds can generate various model hypotheses in the MHTC algorithm. **Fig. 7(c)** shows the probability distribution of an expected cluster–target association between the cluster range measurement appearance and the target's predicted location with Gaussian distributions for the existing targets and the uniform distribution for the new target or false clutters (relevant to Section 4.1.2 and Eq. (14))[9]. **Fig. 7(b)** and **Fig. 7(c)** illustrates the likelihood termand the prior termin Eq. (10) for MAP clustering, respectively. **Fig. 7(d)** shows all possible combinations of the cluster–target associations based on the aforementioned model hypothesis, which can include the case of false measurements, missed detection, and existing target tracking. For all generated model and data association hypotheses, the global hypothesis probability in Eq. (22) was calculated and compared to produce only the *L*-best global hypotheses by Step 6 and 7 in Section 4.4.

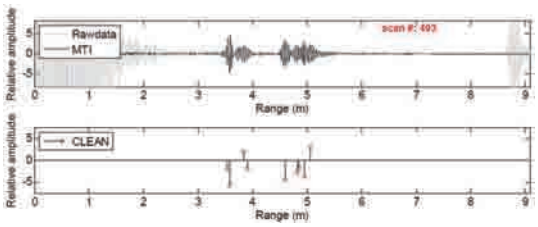

Fig. 7(a)　Preprocessing for scan 493.

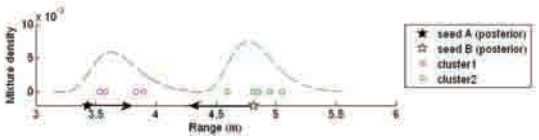

Fig. 7(b)　The MAP EM clustering of the resolved 7 TOAs for the resultant Gamma mixture component distributions.

Fig. 7(c)　The probability distribution of an expected cluster–target association between the cluster range measurement appearance and the target's predicted location with Gaussian distributions and the uniform distribution.

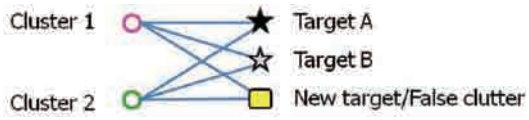

Fig. 7(d)　Possible combinations of the cluster–target associations.

Fig. 7 The processing steps of the MHTC algorithm.

Fig. 8 shows the MHTC result on 572 scans (45 sec recording time) for 3 humans walking randomly in and out of the radar range. For each human target, the a posteriori state estimates of the human target range are plotted as a colored path. To evaluate the performance of the result, LADAR range measurements are overlayed as a reference where the LADAR1 range measurements (coaxial to radar, near side to human from the radar) are shown as the blue band of dots, and the LADAR2 range measurements (far side of human from the radar) are shown as the gray band of dots. Note that when humans change direction, the side of human body faces both LADARs so that the LADARs see a wider cross section with their edges further apart (arm-to-arm depth rather than chest depth) resulting in larger spread of the LADAR measurements bands at such instances (e.g. at 30 sec, 34 sec, 38 sec, 41 sec, and 42 sec). Also, note that the estimated range was mostly in the middle of the blue and gray band in two radar measurements, except in the case when sudden walking direction change introduces the smoothing effect in the KF. Our experiments show that the range accuracy of mono-static UWB radar is nearly as good as LADAR. We can identify different modes over the observation time: (1) no targets until 9 sec; (2) new target track initiation at 9 sec, target A; (3) single human target tracking from 9 sec to 17 sec, target A; (4) target deletion at 17 sec, target A; (5) no targets from 17 sec to 26 sec; (6) target track initiation at 26 sec, target B; (7) single human target tracking from 26 sec to 36 sec, target B; (8) target track initiation at 36 sec, target C; (9) double human target tracking from 36 to the end; and (10) two target crossing at 39 sec and 43 sec, target B and C. The MHTC results shows that the range estimation paths agree the LADAR reference measurements for all different mode and transitions.

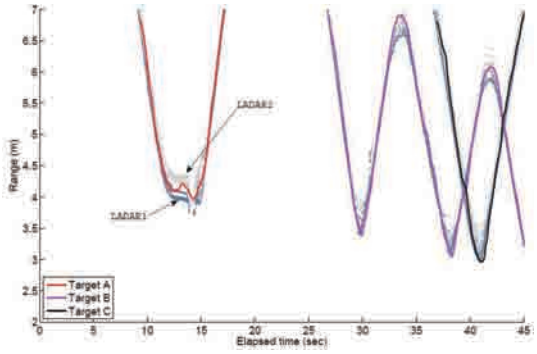

Fig. 8　The MHTC results with changing numbers of human targets.

6.　Discussion and Conclusion

Ultra-Wide-Band radar offers a complementary technology for tracking humans, as it works well in conditions (such as in the dark, or in dusty, foggy, rainy environments) where the performance of other sensing modalities degrades. However, the different nature of the UWB signal requires new processing and tracking algorithms. Based on the novel observation that mono-static UWB radar multipath scatters from walking humans can be modeled as a point process, we developed a rigorous method to track a fixed number of human targets [14]. In this paper we extended this method to handle a variable number of targets, along with clutter and temporary occlusions. This extension is necessary to make our tracking approach applicable to realistic human tracking and detection problems. The key to our extension was the novel formulation of an MHTC procedure which allowed us to rigorously organize and select the complex data associations inherent in UWB multi-path scattering from multiple

targets. Ongoing work seeks to improve our method to identify clutter in the UWB return signal, and to extend the approach to multi-antenna configurations as well as LADAR-and-radar or vision-and-radar multi-modal human tracking techniques.

References

1）M. I. Skolnik (1970) Radar Handbook. McGraw Hill, New York

2）P. Z. Peebles, Jr. (1998) Radar Principles. Wiley, New York

3）R. M. Narayanan (2008) Through-Wall Radar Imaging using UWB Noise Waveforms. In: J. Franklin Institute, vol.345, no. 6, pp. 659-678.

4）C. Chang, and A. Sahai (2004) Object tracking in a 2D UWB sensor network. In: Proc. 38th Asilomar Conf. on Signals, Systems and Computers, vol. 1, pp. 1252-1256

5）R. A. Scholtz, D. M. Pozar, and W. Namgoong (2005) Ultra-Wideband Radio. EURASIP Journal of Applied Signal Processing, no. 3, 2005, pp. 252-272

6）S. Chang, R. Sharan, M. Wolf, N. Mitsumoto, and J.W. Burdick (2009) UWB radar-based tracking of humans. In: Proc. IEEE Radar Con, Pasadena, CA

7）Y. Bar-Shalom and T. E. Fortmann (1988) Tracking and Data Association. Academic Press Inc., Orlando, FL

8）S. S. Blackman and R. Popoli (1999) Design and Analysis of Modern Tracking Systems. Artech House, Norwood, MA

9）G. W. Pulford (2005) Taxonomy of multiple target tracking methods. IEE Proceedings - Radar, Sonar & Navigation, 152(5):291-304

10）E. F. Knott, J. F. Shaeffer, and M. T. Tuley (1993) Radar Cross Section, 2nd ed.. Artech House, Norwood, MA

11）M. Wolf (2008) Target Tracking Using Clustered Measurements, with Applications to Autonomous Brain-Machine Interfaces. In: Ph.D. thesis, Department of Mechanical Engineering, California Institute of Technology, Pasadena, CA

12）B. Lau, K.O. Arras, andd W. Burgard (2009) Tracking Groups of People with a Multi-Model Hypothesis Tracker. In: Proc. IEEE Int. Conf. on Robotics and Automation, May 12-17, 2009, Kobe Japan.

13）H. Hashemi (1993) Impulse response modeling of the indoor radio propagation channels. IEEE Trans. Select. Areas Commun., vol. 11, no. 7

14）S. Chang, N. Mitsumoto, J.W. Burdick (2009) An algorithm for UWB radar-based human detection. In: Proc. IEEE RadarCon, Pasadena, CA

15）S. M. Yano (2002) Investigating the ultra-wideband indoor wireless channel. In: Proc. IEEE VTC Spring Conf., vol. 3, pp. 1200-1204

16）D. B. Reid (1979) An algorithm for tracking multiple targets. IEEE Transactions on Automatic Control, 24(6):843-854.

17）K. G. Murty (1968) An algorithm for ranking all the assignments in order of increasing cost. Operations Research, 16:682-687

18）G. McLachlan and D. Peel (2000) Finite Mixture Models, Wiley Interscience

19）J.L. Beck and K.-V. Yuen (2004)Model Selection Using Response Measurements: Bayesian Probabilistic Approach. J Engineering Mechanics, vol. 130, no. 2, pp. 192-203

＜著　者＞

光本　直樹
（みつもと　なおき）
（株）デンソー　基礎研究所
先端研究，工学博士
人工知能，創発コンピュータ，
脳科学応用の研究に従事

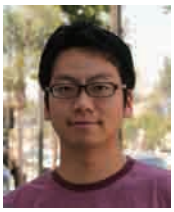

SangHyun Chang
サムソンエレクトロニクス
（韓国）PhD
レーダー信号処理，アンテナ技
術の研究に従事

Michael Wolf
ジェット推進研究所（米国）
PhD
ロボット制御，生体信号解析，
物体追跡，確率信号処理の研
究に従事

Joel W. Burdick
カリフォルニア工科大学（米
国）　教授　PhD
ロボティクス，ニューロモー
フィック，自動運転の研究に
従事